Analysis of Backward Euler Method in Presence of Saturation Nonlinearity and Applications in Power Systems Simulation

Soumyajit Gangopadhyay and Nilanjan Ray Chaudhuri

***Abstract*— Dynamic simulation of a power system involves the solutions of many nonlinear differential-algebraic equations that are computationally expensive. While quasi steady state approximation methods are computationally efficient, they cannot capture many power system phenomena such as controller-induced instabilities. Recently, Backward Euler Method (BEM) has been used to produce a coarser approximation of the ground truth (obtained from Trapezoidal method) at a lower computational effort. However, no fundamental analysis exists in the literature for understanding the properties of BEM in presence of saturation nonlinearity in a dynamical system. This paper mathematically investigates the properties of BEM when applied to a $1-$dimensional and a $2-$ dimensional system with saturation nonlinearity. Our analyses show that besides hyper-stability, unlike in a linear time-invariant system, BEM can also suffer from hyperinstability in a system with saturation. Based on the mathematical analyses, qualitative recommendations are presented for adaptively varying the stepsizes of BEM such that the solution can resemble the ground truth in an averaged sense at a significantly lower computational cost. BEM with adaptive stepsize variation is applied to simulate (i) a single-generator system (with saturation nonlinearity in the governor's dynamics) feeding a standalone load and (ii) a 6-bus system with a synchronous generator and inverter-based resources having saturation nonlinearity. It is shown that by adaptively varying the stepsizes based on the presented recommendations, BEM can produce the same end result as in the ground truth while consuming significantly less cpu time.**

I. INTRODUCTION

Simulation of power system dynamic models is necessary to conduct several studies during offline planning and online operations including long term voltage stability assessment (offline), cascading failure simulation (offline) and dynamic security assessment (online). Such simulations require the solutions of many nonlinear differential-algebraic equations (DAEs) that are augmented with a discrete variable z as shown in (1)-(3).

$$\dot{x} = f(x, V, z) \tag{1}$$

$$0 = I(x, V, z) - Y_N(z)V \tag{2}$$

$$0 \succ h(x, V, z) \tag{3}$$

The variable $x \in \mathbb{R}^n$ is the state vector, $V \in \mathbb{R}^m$ represents the vector containing the real and the imaginary components of the bus voltages, $z \in \mathbb{Z}^p$ is an implicit variable whose entries are either 0 or 1 that indicate the status of the circuit breakers operated by the relays, $I \in \mathbb{R}^m$ represents the real and the imaginary components of the current injection in the buses, $Y_N \in \mathbb{R}^{m\times m}$ is the admittance matrix of the network in its real form (i.e., separating the real and the imaginary parts of the equations) and $h : \mathbb{R}^n \times \mathbb{R}^m \times \mathbb{Z}^p \to \mathbb{R}^q$ models the constraints that define the operation of the relays.

Given the initial conditions $(x_0, V_0, z_0) \in \mathbb{R}^n \times \mathbb{R}^m \times \mathbb{Z}^p$ at time $t = 0$, the objective of dynamic simulation is to determine x and V over a simulation period. Note that z is an implicit variable that changes only when (3) is violated. Hence, unless (3) is violated which otherwise can bring in discontinuities (see [1] on handling discontinuities), dynamic power system simulation involves finding the solutions of the DAEs of the form (1)-(2).

DAEs of the form (1)-(2) can be solved using implicit numerical integration methods that transform the ordinary differential equations (ODEs) of the form (1) into algebraic equations at each time step of the numerical simulation and then the resulting set of nonlinear algebraic equations is solved along with (2) at each time step using nonlinear solvers. To this end, different implicit numerical integration methods have been proposed in literature [2] for accurate time domain simulation of power systems. Among these techniques, the trapezoidal method (TM) is widely used for accurate simulation of power system dynamic models (referred as '*ground truth*' in this paper). However, accurate simulation of power system dynamic models involves a significant computational burden, which often limits the application of the existing numerical methods for online studies such as dynamic security assessment (DSA) of power systems. Due to the several possible combinations, this massive computational effort poses an obstacle even for offline contingency studies such as $N-k$ contingencies when k is relatively large. This is relevant for cascading failure simulations where the initiating failure size k is larger than 2. The problem is further exacerbated in modern power grids with growing inverter-based resources (IBRs) that give rise to a significant increase in dynamic states and numerical stiffness. This motivates the need for faster simulation of dynamic models of power systems.

To enable long-term voltage-stability analysis and statistical analysis of cascading failure, Quasi Steady State (QSS) approximation of the full dynamic model of a power system has been proposed in the literature. While computationally efficient, the limitations of QSS approximation are two-fold. Firstly, typical AC-QSS models [3] fail to capture the voltage threshold-based undervoltage load shedding (UVLS) relays in practical systems [4], [5] since most of the time, the models cannot generate an equilibrium below the voltage threshold due to divergence. Therefore, such models may produce completely different results from the ground truth. Secondly, AC-QSS models cannot capture angle, frequency, and controller-induced instabilities.

Instead of simulating a simplified model obtained by QSS approximation of the full dynamic model that suffers from the aforementioned limitations, producing a coarse approxi-

Financial support from NSF Grant Award ECCS 1836827 is gratefully acknowledged. Soumyajit Gangopadhyay, and Nilanjan Ray Chaudhuri are with The School of Electrical Engineering Computer Science, The Pennsylvania State University, University Park, PA, 16802, USA. szg6052@psu.edu, nuc88@psu.edu

mation that neglects the finer details of the ground truth can be sufficient in many applications. For example, accurate tracking of the electromechanical oscillations may not be of significant interest during long term voltage stability assessment or cascading failure studies. Similarly for DSA, typically $(N-1)$ contingency is studied and it suffices if it can indicate the stability of the post-disturbance condition and any impending relay actions after 20-30 s. In summary, accuracy can be partially compromised in multiple applications which in turn can be exploited to obtain simulation speedup. While less accurate than the detailed simulation of the full dynamic model, this approach does not suffer from the above limitations, thus outperforming the QSS method.

Backward Euler Method (BEM) is an implicit integration method that can enable faster dynamic simulation of power systems, thanks to its stiff decay property [6]. The stiff decay property of BEM allows itself to ignore the oscillations in the ground truth by adopting large time steps during the simulation. At the same time, BEM can significantly preserve the coarser information contained in the ground truth. As a consequence, the advantages obtainable from the application of BEM in dynamic simulation of power systems are twofold. First, it can significantly reduce the computational burden associated with the accurate simulation of the full dynamic model of power systems. Second, BEM can track the response of a power system in an averaged sense which lends itself to a variety of power system studies. Due to these advantages, BEM has been used in [7], [8] for fast cascading failure simulation of power system dynamic models.

However, to the best of our knowledge, no fundamental analysis exists in literature for understanding the properties of BEM in presence of saturation nonlinearity in a dynamical system. Saturation nonlinearity is often observed in power systems, for example, in dc side current limitation of IBRs and their ac-side current control, and also in the automatic voltage regulator (AVR), the power system stabilizer (PSS), and the governor in synchronous generators. Hence, investigations on the application of BEM for faster simulation of power systems in the presence of saturation nonlinearity requires immediate attention.

The key contributions of this paper are:

- Analytical treatment is presented to analyze the properties of BEM when applied to a 1- and a 2-dimensional dynamical system with saturation nonlinearity.
- Based upon the mathematical insights, *qualitative* recommendations for adapting the time steps of BEM are presented.
- Case studies on power system dynamic models with SGs and IBRs highlight the validity of our analysis.

II. Overview of BEM

BEM is a one-step, implicit, first-order numerical integration method that discretizes an ODE of the form (1) to form an algebraic equation of the form

$$x_{n+1} = x_n + hf(x_{n+1}, V_{n+1}) \tag{4}$$

Once discretized, (4) is solved along with (5) to obtain the solutions x_{n+1} and V_{n+1} at time $t = t_{n+1}$.

$$I(x_{n+1}, V_{n+1}) - Y_N V_{n+1} = 0 \tag{5}$$

In (4), $h > 0$ is the time step used to discretize (1) such that $h = t_{n+1} - t_n \ \forall n \in \mathbb{Z}_{\geq 0}$ and $t_0 = 0$ is the starting time of the simulation. Since z is an implicit variable, we have not explicitly shown the dependence of f, I and Y_N on z in (4) and (5) along with the rest of this paper.

A. Newton's iterations

Determining x_{n+1} and V_{n+1} at $t = t_{n+1}$ requires solving the nonlinear algebraic equations given by (4) and (5). Typically, the Newton's method is used for this purpose. At the $(k+1)^{th}$ iteration corresponding to $t = t_{n+1}$, the mismatch is calculated as

$$m_{n+1}^{(k+1)} = \begin{bmatrix} x_{n+1}^{(k)} - x_n - hf(x_{n+1}^{(k)}, V_{n+1}^{(k)}) \\ I(x_{n+1}^{(k)}, V_{n+1}^{(k)}) - Y_N V_{n+1}^{(k)} \end{bmatrix} \tag{6}$$

where $x_{n+1}^{(0)}$ and $V_{n+1}^{(0)}$ are the initial guesses of the solutions at $t = t_{n+1}$. Then, the update vector is calculated as

$$\begin{bmatrix} \Delta x_{n+1}^{(k)} \\ \Delta V_{n+1}^{(k)} \end{bmatrix} = -(J_{n+1}^{(k)})^{-1}(m_{n+1}^{(k+1)}) \tag{7}$$

where $J_{n+1}^{(k)}$ is the Jacobian matrix at the $(k+1)^{th}$ iteration corresponding to $t = t_{n+1}$. The solution is then updated as

$$\begin{bmatrix} x_{n+1}^{(k+1)} \\ V_{n+1}^{(k+1)} \end{bmatrix} = \begin{bmatrix} x_{n+1}^{(k)} \\ V_{n+1}^{(k)} \end{bmatrix} + \begin{bmatrix} \Delta x_{n+1}^{(k)} \\ \Delta V_{n+1}^{(k)} \end{bmatrix} \tag{8}$$

This process is stopped when $||m_{n+1}^{(\gamma)}||_\infty < \epsilon$ at some iteration γ where $\epsilon > 0$ is the tolerance for convergence.

B. Absolute stability property

To assess the absolute stability property of BEM, the standard approach is to consider the test equation $\dot{x} = \lambda x$ where λ is a complex number. The absolute stability region of BEM is the region in the complex $h\lambda$ plane such that if BEM is used to solve the test equation with $h\lambda$ belonging to this region, then $|x_{n+1}| \leq |x_n| \ \forall n \in \mathbb{Z}_{\geq 0}$. By applying (4) to the test equation, we obtain $x_{n+1} = \frac{1}{1-h\lambda} x_n$. Hence, the absolute stability region of BEM is the entire left half of $h\lambda$ plane in addition to the portion of the right half plane that lies outside the unit circle centered at $(1, 0)$. Since the absolute stability region of BEM contains the entire left half of the $h\lambda$ plane, BEM is *A-stable* [6].

C. Stiff decay property and Hyperstability

If $h \to \infty$, then $|\frac{1}{1-h\lambda}| \to 0$ and hence it can be concluded from section II-B that $|x_{n+1}| \to 0$. This property of BEM is called the stiff decay property. The stiff decay property of BEM implies that if BEM is used with large time steps, then BEM can ignore the oscillations in the ground truth (if any) while converging to the equilibrium of the system. As a consequence, if the ground truth has stable and decaying oscillations, then BEM can converge to the stable equilibrium. Thus, BEM can produce the same end result as in the ground truth at a lower computational cost. Hence, unless the stable oscillations in the ground truth are of practical interests, BEM can be a promising method for faster simulation of power system dynamic models represented by DAEs of the form (1)-(2). However, if the ground truth has unstable oscillations (i.e., when $Re(\lambda) > 0$), then stiff decay implies that BEM converges to the unstable equilibrium. Thus, BEM fails to capture the instability of the ground truth when the stepsize used in the numerical simulation

exceeds a certain value. Popularly known as hyperstability, this is a major drawback associated with BEM since it prevents the adoption of large time steps (which is required to obtain simulation speedup) when the ground truth has unstable oscillations. It can be mathematically shown that the hyperstability situation can be avoided by choosing a stepsize that is less than $h_M = \frac{2Re(\lambda)}{|\lambda|^2}$.

III. Application of BEM in dynamical systems with saturation nonlinearity

A. One-dimensional system

Consider the one-dimensional system

$$\dot{x} = \lambda c \text{ sat}\left(\frac{x}{c}\right) \tag{9}$$

where $x \in \mathbb{R}$, $\lambda \in \mathbb{R} \setminus \{0\}$ and $c > 0$. The sat$(\cdot)$ function is defined as:

$$\text{sat}(u) := \begin{cases} u & \text{if } |u| < 1 \\ \text{sgn}(u) & \text{if } |u| \geq 1 \end{cases} \tag{10}$$

where sgn(x) represents the signum function. The discretization of (9) using BEM gives

$$x_{n+1} = x_n + h\lambda c \text{ sat}\left(\frac{x_{n+1}}{c}\right) \tag{11}$$

where x_{n+1} is the solution obtained from BEM at $t = t_{n+1}$.

Proposition III.1: *The origin of* (9) *is globally asymptotically stable if and only if* $\lambda < 0$.

Proof: **Necessity:** Global asymptotic stability implies local asymptotic stability which implies $\lambda < 0$.

Sufficiency: Define $V(x) = \frac{1}{2}x^2 \ \forall x \in \mathbb{R} \setminus 0$. Then, $\dot{V}(x) = x\dot{x} = \lambda c x \text{sat}\left(\frac{x}{c}\right)$. Clearly, if $\lambda < 0$, then $\dot{V}(x) < 0 \ \forall x \setminus \{0\}$. Thus, the origin of (9) is globally asymptotically stable. ■

Proposition III.2: *BEM converges to the origin for all admissible stepsizes* $h > 0$ *if* $\lambda < 0$ *in* (9).

Proof: It is known from the existing literature on BEM [9] that if there exists a quadratic Lyapunov function $V(x)$ that satisfies $\dot{V}(x) < 0$ along the trajectory of the ground truth $\forall t \geq 0$, then the solution from BEM satisfies $V(x_{n+1}) < V(x_n)$ for all admissible stepsizes $h > 0$. If $\lambda < 0$, $V(x) = \frac{1}{2}x^2$ is a quadratic Lyapunov function of (9). ■

From Proposition III.2., it can be concluded that if $x_n > 0$, then $x_{n+1} < x_n$ for all admissible stepsizes $h > 0$. Further analysis can be conducted to show that if $x_n > 0$, then $x_{n+1} > 0$. Thus, if $x_n > 0$, then $0 < x_{n+1} < x_n$. Similarly, if $x_n < 0$, then $x_n < x_{n+1} < 0$. Thus, BEM can produce a numerical solution that is qualitatively similar to the ground truth for all admissible stepsizes $h > 0$.

Proposition III.3. *Assume* $\lambda > 0$, $0 < h\lambda < 1$. *Then,* $x_n > 0 \implies x_{n+1} > x_n$. *Similarly,* $x_n < 0 \implies x_{n+1} < x_n$

Proof: Suppose $x_n > 0$. Then, $x_{n+1} > h\lambda c \ sat(x_{n+1}/c)$ (from (11)). Hence, $x_{n+1} \neq 0$. This implies $\frac{x_{n+1}}{c \ sat(x_{n+1}/c)} \geq 1$. Now, $x_{n+1} < 0 \implies 1 \leq \frac{x_{n+1}}{c \ sat(x_{n+1}/c)} < h\lambda \implies h\lambda > 1$ which contradicts our assumption. Hence $x_{n+1} > 0$ which further implies $x_{n+1} > x_n$ (from (11)). Similar reasoning can be used to prove that $x_n < 0 \implies x_{n+1} < x_n$ ■

Thus, $h < \frac{1}{\lambda}$ is a sufficient condition for BEM to track the instability of the ground truth corresponding to $\lambda > 0$.

Proposition III.4. *Assume* $\lambda > 0$. *Once BEM enters positive saturation (i.e.,* $x_n \geq c$ *but* $x_{n-1} < c$*) or negative saturation (i.e.,* $x_n \leq -c$ *but* $x_{n-1} > -c$*), the instability of the ground truth can be captured by selecting* h *that satisfies* $h\lambda > 1$ *provided the solution from the last step is used to initialize the solution at the current step, i.e.,* $x_{n+1}^{(0)} = x_n$.

Proof: Assume BEM has entered positive saturation. Then, the initial mismatch at the current step $m_{n+1}^{(1)} = -h\lambda c$ and $J_{n+1}^{(0)} = 1$. Hence, $x_{n+1}^{(1)} = x_n + h\lambda c$. This implies $m_{n+1}^{(2)} = x_{n+1}^{(1)} - x_n - h\lambda c \text{ sat}(\frac{x_{n+1}^{(1)}}{c}) \implies m_{n+1}^{(2)} = 0$. Thus, $x_{n+1} = x_n + h\lambda c > x_n$. Similarly, if we assume that BEM has entered negative saturation, then it can be proved that $x_{n+1} = x_n - h\lambda c < x_n$. Thus, when $\lambda > 0$, once BEM enters the positive/negative saturation region, the solution at *any* future time (and hence any $h > 0$ is admissible) will be greater/less than x_n, respectively, if the solution is initialized with the solution from the last time step. As a consequence, once BEM hits saturation, a higher value of h satisfying $h\lambda > 1$ can be adopted to obtain simulation speedup without failing to capture the instability of the ground truth. ■

B. Two-dimensional system

Consider the two-dimensional system

$$[\dot{x}_1 \quad \dot{x}_2]^T = A \begin{bmatrix} c \text{ sat}\left(\frac{x_1}{c}\right) & x_2 \end{bmatrix}^T \tag{12}$$

where $x_1, x_2 \in \mathbb{R}$, $A \in \mathbb{R}^{2\times 2}$ such that A is invertible and $c > 0$. We use $x_n = [x_1 \quad x_2]_n^T$ to denote the output of BEM at $t = t_n$. Then, discretization of (12) using BEM gives

$$x_{n+1} = x_n + hA \begin{bmatrix} c \text{ sat}\left(\frac{x_1}{c}\right) & x_2 \end{bmatrix}_{n+1}^T \tag{13}$$

Proposition III.5. *If BEM converges, then* $\lim_{n\to\infty} x_n = \mathbf{0}$, *where* $\mathbf{0}$ *represents the origin.*

Proof: From (13), we can conclude that if BEM converges, then $\lim_{n\to\infty} A \begin{bmatrix} c \text{ sat}\left(\frac{x_1}{c}\right) & x_2 \end{bmatrix}_n^T = \mathbf{0} \implies \lim_{n\to\infty} \begin{bmatrix} c \text{ sat}\left(\frac{x_1}{c}\right) & x_2 \end{bmatrix}_n^T = \mathbf{0} \implies \lim_{n\to\infty} x_n = \mathbf{0}$ ■

It is seen from (13) that if x_{n+1} is in the linear region (i.e., if $-c < (x_1)_{n+1} < c$), then $x_{n+1} = (I - hA)^{-1}x_n$ provided $h \neq \frac{1}{\lambda(A)}$ where $\lambda(A)$ is an eigenvalue of A.

Proposition III.6. *Suppose* $a_{22} \neq 0$. *Then the origin of* (12) *is globally asymptotically stable if and only if* A *is Hurwitz and* $a_{22} < 0$ *(where* a_{ij} *is the element in the* i^{th} *row and the* j^{th} *column of* A*).*

Proof: **Necessity:** Global asymptotic stability implies local asymptotic stability $\implies$ A is Hurwitz. We prove $a_{22} < 0$ by contradiction. Assume that $a_{22} > 0$. Now, construct an initial condition $x_0 = [c \quad \frac{-a_{21}c}{a_{22}}]^T$. Since $\frac{|A|}{a_{22}} > 0$, $\dot{x_1} > 0$ and $\dot{x_2} = 0 \ \forall t \geq 0$. Consequently, $\lim_{t\to\infty} x_1 = \infty$, thus contradicting global asymptotic stability. Hence $a_{22} < 0$.

Sufficiency: Given A is Hurwitz and $a_{22} < 0$, we find a Lyapunov function $V(x)$ to prove the global asymptotic stability of the origin. In particular, we use the variable gradient method. The idea is to choose $g(x)$ such that $g(x)$ is the gradient of a positive definite scalar function $V(x)$ and $\dot{V}(x)$ is negative definite. Suppose $g(x) = [\alpha(x)x_1 + \beta(x)x_2 \quad \gamma(x)x_1 + \delta(x)x_2]^T$. For $g(x)$ to be the gradient of a scalar function, we want $\frac{\partial g_i}{\partial x_j} = \frac{\partial g_j}{\partial x_i} \ \forall i, j \in \{1, 2\}$. Hence, we must ensure

$$\beta(x) + \frac{\partial \alpha(x)}{\partial x_2}x_1 + \frac{\partial \beta(x)}{\partial x_2}x_2 = \gamma(x) + \frac{\partial \gamma(x)}{\partial x_1}x_1 + \frac{\partial \delta(x)}{\partial x_1}x_2 \tag{14}$$

Since $g(x) = \nabla V(x)$, $\dot{V}(x) = g(x)^T\dot{x} = (\alpha(x)a_{11} + \gamma(x)a_{21})x_1 c \text{ sat}\left(\frac{x_1}{c}\right) + (\beta(x)a_{12} + \delta(x)a_{22})x_2^2 + (\alpha(x)a_{12}x_1 + \beta(x)a_{11}c \text{ sat}\left(\frac{x_1}{c}\right) + \gamma(x)a_{22}x_1 + \delta(x)a_{21}c \text{ sat}\left(\frac{x_1}{c}\right))x_2$. To cancel the cross product terms, we choose $\alpha(x)a_{12}x_1 + \beta(x)a_{11}c \text{ sat}\left(\frac{x_1}{c}\right) + \gamma(x)a_{22}x_1 + \delta(x)a_{21}c \text{ sat}\left(\frac{x_1}{c}\right) = 0$ so that $\dot{V}(x) = (\alpha(x)a_{11} + \gamma(x)a_{21})x_1 c \text{ sat}\left(\frac{x_1}{c}\right) + (\beta(x)a_{12} + \delta(x)a_{22})x_2^2$. We further choose $\beta(x) = \beta =$ constant, $\gamma(x) = \gamma =$ constant and $\delta(x) = \delta =$ constant so that $\alpha(x)$ depends only on x_1. In particular, $\alpha(x) = \frac{-\gamma a_{22}}{a_{12}} - \left(\frac{\beta a_{11} + \delta a_{21}}{a_{12}}\right)\frac{c \text{ sat}\left(\frac{x_1}{c}\right)}{x_1}$. Then, from (14), $\beta = \gamma$. Now, $V(x)$ can be obtained as

$$V(x) = \int_0^{x_1}\left(-\left(\frac{\gamma a_{11} + \delta a_{21}}{a_{12}}\right)c \text{ sat}\left(\frac{y_1}{c}\right) - \frac{\gamma a_{22}}{a_{12}}y_1\right)dy_1 + \int_0^{x_2}(\gamma x_1 + \delta y_2)dy_2$$

$$\implies V(x) = \frac{1}{2}x^T P x + K\int_0^{x_1} c \text{ sat}\left(\frac{y}{c}\right)dy \tag{15}$$

where $P = \begin{bmatrix} \frac{-\gamma a_{22}}{a_{12}} & \gamma \\ \gamma & \delta \end{bmatrix}$ and $K = -\frac{\gamma a_{11} + \delta a_{21}}{a_{12}}$. We need to choose γ and δ such that

$$\frac{-\gamma a_{22}}{a_{12}} > 0,\ \frac{-\gamma a_{22}\delta}{a_{12}} - \gamma^2 = \frac{-\gamma a_{22}}{a_{12}}(\delta + \frac{\gamma a_{12}}{a_{22}}) > 0,\ K \geq 0 \tag{16}$$

$$\gamma a_{12} + \delta a_{22} < 0,\ \ \alpha(x)a_{11} + \gamma a_{21} < 0 \tag{17}$$

From (16), we conclude that γ and a_{12} must be of same sign (since $a_{22} < 0$). Additionally, $\delta > \frac{-\gamma a_{12}}{a_{22}}$. Hence, $\delta > 0$. We choose $\delta = \frac{-\gamma a_{12}}{a_{22}} + \frac{(a_{11}+a_{22})|A|}{a_{22}}$. Then, if $a_{12} < 0$, we choose $\gamma < -a_{11}a_{21}$ such that the chosen γ and a_{12} are of same sign. On the other hand, if $a_{12} > 0$, we choose $\gamma > -a_{11}a_{21}$ such that the chosen γ and a_{12} are of same sign. With these choice of γ and δ, it is possible to show that (16)-(17) are satisfied. Note that $V(x)$ in (15) is radially unbounded, which is defined $\forall x \in \mathbb{R}^2$ if $a_{12} \neq 0$. Hence, if $a_{12} = 0$, the global asymptotic stability cannot be proved using $V(x)$ given by (15). However, if $a_{12} = 0$, then $a_{11} < 0$ (since A is Hurwitz). Hence $\lim_{t\to\infty} x_1 = 0$ (see the proof of Proposition III.1.). This further implies $\lim_{t\to\infty} x_2 = 0$ (since $a_{22} < 0$). ■

It can be concluded from Proposition III.6. that unlike in a linear time-invariant system, A being Hurwitz is necessary but not sufficient for global asymptotic stability of origin.

Proposition III.7. *BEM converges for all admissible stepsizes $h > 0$ if A is Hurwitz, $a_{22} < 0$ and $a_{12}a_{21} \geq 0$.*

Proof: Besides A being Hurwitz and $a_{22} < 0$, if $a_{12}a_{21} > 0$, then the variable K in (16) can be set to zero while satisfying (16)-(17). As a consequence, $V(x)$ becomes quadratic which implies the convergence of BEM for all admissible stepsizes $h > 0$ (see the reasoning in the proof of Proposition III.2.). Further, if $a_{12}a_{21} = 0$, then the proof of the convergence of BEM for all admissible stepsizes $h > 0$ is trivial. ■

Proposition III.8. *If x_0 is in linear region, then as $h \to \infty$, BEM converges $\forall A \in \mathbb{R}^{2\times 2}$ and $\forall\, c > 0$.*

Proof: The mismatch at the 1^{st} iteration corresponding to $t = t_1$ can be written as $m_1^{(1)} = x_1^{(0)} - x_0 - hA\left(\begin{bmatrix} c \text{ sat}\left(\frac{x_1}{c}\right) & x_2 \end{bmatrix}_1^T\right)^{(0)}$ We use x_0 to initialize x_1 i.e. $x_1^{(0)} = x_0$. Since x_0 is in linear region, $x_1^{(0)}$ is in linear region and hence $\left(\begin{bmatrix} c \text{ sat}\left(\frac{x_1}{c}\right) & x_2 \end{bmatrix}_1^T\right)^{(0)} = x_1^{(0)} = x_0$. Thus $m_1^{(1)} = -hAx_0$. The Jacobian at the $(k+1)^{th}$ iteration corresponding to $t = t_1$ can be written as

$$J_1^{(k)} = I - hAG_1^{(k)}$$

where

$$G_1^{(k)} = \begin{cases} I & \text{if } x_1^{(k)} \text{is in linear region} \\ \begin{bmatrix} 0 & 0 \\ 0 & 1 \end{bmatrix} = G_{sat} & \text{if } x_1^{(k)} \text{ is in saturation region} \end{cases}$$

Since $x_1^{(0)}$ is in linear region, $G_1^{(0)} = I$ and hence $J_1^{(0)} = I - hA$. So, $\Delta x_1^{(0)} = -(J_1^{(0)})^{-1}(m_1^{(1)}) = (J_1^{(0)})^{-1}(hAx_0) \implies x_1^{(1)} = x_0 + \Delta x_1^{(0)} = x_0 + (I - hA)^{-1}(hAx_0) = (I - hA)^{-1}x_0$. Note that if $h \to \infty$, then $(I - hA)^{-1}x_0 \to \mathbf{0}\ \forall A \in \mathbb{R}^{2\times 2}$. Hence, $x_1^{(1)}$ belongs to the linear region $\forall c > 0$. Consequently, $\begin{bmatrix} c \text{ sat}\left(\frac{x_1}{c}\right) & x_2 \end{bmatrix}_1^T)^{(1)} = x_1^{(1)}$. So, $m_1^{(2)}$ becomes

$$m_1^{(2)} = x_1^{(1)} - x_0 - hAx_1^{(1)} = (I - hA)x_1^{(1)} - x_0 = \mathbf{0}$$

Since $m_1^{(2)} = \mathbf{0}$, BEM converges to the origin. ■

We conclude from Proposition III.8. that if x_0 is in linear region, then for a given $A \in \mathbb{R}^{2\times 2}$ and $c > 0$, there exists a lower bound on h such that BEM converges when a value of h exceeding the lower bound is used in simulation. Hence BEM suffers from hyperstability when x_0 is in linear region. Let $h_L(A, c) > 0$ be the minimum value of h such that $\forall h \geq h_L(A, c)$, the set L is $(I - hA)^{-1}$invariant where L is the linear region defined by $L := \{(x_1, x_2) : -c < x_1 < c, x_2 \in \mathbb{R}\}$. Then, for a given A and $c > 0$, selecting $h \geq h_L(A, c)$ ensures that BEM never enters the saturation region when x_0 is in linear region. As a consequence, when x_0 is in linear region, BEM cannot capture the instability of the ground truth (if any) if $h \geq h_L(A, c)$. Hence, it is necessary to choose $h < h_L(A, c)$ in order to capture the instability of the ground truth (if any). However, when A has at least one eigenvalue with positive real part (indicating the ground truth is unstable), the sufficient condition to avoid hyperstability for the system (13) is given by $h < \max\{\frac{2Re(\lambda_i)}{|\lambda_i|^2}\}$ where λ_i is the i^{th} eigenvalue of $A\ \ \forall i \in \{1, 2\}$. On the other hand, when A is Hurwitz, it is non-trivial to determine the sufficient condition on h required for avoiding hyperstability.

Proposition III.9. Consider the statements (a)-(d):
(a) $\frac{|A|}{a_{22}} > 0$
(b) $|A| < 0$ and $a_{22} = 0$
(c) $\frac{|A|}{a_{22}} < 0$
(d) $|A| > 0$ and $a_{22} = 0$

(i) Suppose either (a) or (b) holds. Then, BEM produces an unstable response as $h \to \infty$ if x_0 is in saturation region. In particular, if x_0 is in positive saturation, then $\lim_{h\to\infty} x_1 = \begin{bmatrix} \infty & \frac{-a_{21}c}{a_{22}} \end{bmatrix}^T$. Similarly, if x_0 is in negative saturation, then $\lim_{h\to\infty} x_1 = \begin{bmatrix} -\infty & \frac{a_{21}c}{a_{22}} \end{bmatrix}^T$.
(ii) Suppose x_0 is in the saturation region. Then, BEM

converges as $h \to \infty$ if and only if either (c) or (d) holds.

Proof: (i) Assume x_0 is in the positive saturation region. The mismatch at the 1^{st} iteration corresponding to $t = t_1$ can be written as $m_1^{(1)} = x_1^{(0)} - x_0 - hA\left(\begin{bmatrix} c \text{ sat}\left(\frac{x_1}{c}\right) & x_2 \end{bmatrix}_1^T\right)^{(0)}$ We use x_0 to initialize x_1 i.e., $x_1^{(0)} = x_0$. Since x_0 is in the positive saturation region, $\left(\begin{bmatrix} c \text{ sat}\left(\frac{x_1}{c}\right) & x_2 \end{bmatrix}_1^T\right)^{(0)} = \begin{bmatrix} c & (x_2)_0 \end{bmatrix}^T$. Thus $m_1^{(1)} = -hA\begin{bmatrix} c & (x_2)_0 \end{bmatrix}^T$. Since $x_1^{(0)}$ is in the positive saturation region, $G_1^{(0)} = G_{sat}$ and hence $J_1^{(0)} = I - hAG_{sat}$. So, $\Delta x_1^{(0)} = -(J_1^{(0)})^{-1}(m_1^{(1)}) = (J_1^{(0)})^{-1}(hA\begin{bmatrix} c & (x_2)_0 \end{bmatrix}^T)$ Therefore,

$$\begin{aligned} x_1^{(1)} &= x_1^{(0)} + (J_1^{(0)})^{-1}hA\begin{bmatrix} c & (x_2)_0 \end{bmatrix}^T \\ &= x_0 + (I - hAG_{sat})^{-1}hA\begin{bmatrix} c & (x_2)_0 \end{bmatrix}^T \\ &= x_0 + hA(I - hG_{sat}A)^{-1}\begin{bmatrix} c & (x_2)_0 \end{bmatrix}^T \\ &= x_0 + hA\begin{bmatrix} 1 & 0 \\ \frac{ha_{21}}{1-ha_{22}} & \frac{1}{1-ha_{22}} \end{bmatrix}\begin{bmatrix} c \\ (x_2)_0 \end{bmatrix} \end{aligned}$$

$$\implies (x_1)_1^{(1)} = (x_1)_0 + h\left(a_{11}c + a_{12}\left(\frac{ha_{21}c + (x_2)_0}{1 - ha_{22}}\right)\right)$$

$$\text{and } (x_2)_1^{(1)} = (x_2)_0 + h\left(a_{21}c + a_{22}\left(\frac{ha_{21}c + (x_2)_0}{1 - ha_{22}}\right)\right)$$

Further simplification gives $(x_1)_1^{(1)} = (x_1)_0 + \frac{h(a_{11}c + a_{12}(x_2)_0) - h^2|A|c}{1-ha_{22}}$ and $(x_2)_1^{(1)} = \frac{(x_2)_0 + a_{21}hc}{1-ha_{22}}$. As $h \to \infty$, $(x_2)_1^{(1)} \to \frac{-a_{21}c}{a_{22}}$ and $(x_1)_1^{(1)} \to \infty$ (since either (a) or (b) holds). Thus $(x_1)_1^{(1)} > c$. Hence, $m_1^{(2)}$ becomes

$$\begin{aligned} m_1^{(2)} &= x_1^{(1)} - x_0 - hA\begin{bmatrix} c & (x_2)_1^{(1)} \end{bmatrix}^T \\ &= hA\left(\begin{bmatrix} c & \frac{ha_{21}c + (x_2)_0}{1-ha_{22}} \end{bmatrix}^T - \begin{bmatrix} c & (x_2)_1^{(1)} \end{bmatrix}^T\right) = \mathbf{0} \end{aligned}$$

Since $m_1^{(2)} = 0$ the solution obtained from BEM at $t = t_1$ is $x_1 = \begin{bmatrix} \infty & \frac{-a_{21}c}{a_{22}} \end{bmatrix}^T$. Similarly, it can be shown that if x_0 is in the negative saturation region, then the solution obtained from BEM at $t = t_1$ is $x_1 = \begin{bmatrix} -\infty & \frac{a_{21}c}{a_{22}} \end{bmatrix}^T$. ■

(ii) **Necessity:** Since BEM converges as $h \to \infty$, $\lim_{h\to\infty} \frac{h(a_{11}c + a_{12}(x_2)_0) - h^2|A|c}{1-ha_{22}} \neq \infty$ (see proof of Proposition III.9.(i)). Hence, either (c) or (d) holds.

Sufficiency: We prove this by contradiction. Suppose x_0 is in the positive saturation region. Further, assume that as $h \to \infty$, the system is in the positive saturation region $\implies c \text{ sat}(\frac{(x_1)_1}{c}) = c$. Assuming (c) holds, then, from (13), $\lim_{h\to\infty}(x_1)_1 = \lim_{h\to\infty}((x_1)_0 + hc\frac{|A|}{a_{22}}) < 0$. Hence the system cannot be in the positive saturation region. Assuming (d) holds, $\lim_{h\to\infty}(x_1)_1 = \lim_{h\to\infty}((x_1)_0 + h(a_{11}c + a_{12}(x_2)_0) + h^2a_{12}a_{21}c) < 0$. Hence the system cannot be in the positive saturation region. Similar contradiction can be shown if it is assumed that the system is in the negative saturation region as $h \to \infty$ while x_0 belongs to the positive saturation region. Hence, we conclude that as $h \to \infty$, the system must be in linear region $\implies \lim_{h\to\infty} x_1 = \lim_{h\to\infty}(I - hA)^{-1}x_0 = \mathbf{0}$. Thus, BEM converges. Similar reasoning can be used to prove the convergence of BEM if x_0 is in the negative saturation region. ■

We conclude from Proposition III.9.(i) that if x_0 is in saturation region, then for a given $A \in \mathbb{R}^{2\times2}$ satisfying either (a) $\frac{|A|}{a_{22}} > 0$ or (b) $|A| < 0$ and $a_{22} = 0$, there exists a lower bound on h such that BEM produces an unstable solution when a value of h exceeding the lower bound is used in the simulation. This motivates the following definition of hyperinstability.

Definition III.1. (Hyperinstability of BEM) *In this paper, hyperinstability is defined as a condition where adoption of a stepsize higher than a certain value results in an unstable solution from BEM, despite the ground truth being stable.*

Given the definition of hyperinstability, we conclude that if x_0 is in saturation region and if either (a) $\frac{|A|}{a_{22}} > 0$ or (b) $|A| < 0$ and $a_{22} = 0$ holds, then BEM suffers from hyperinstability. It is worth noting from Proposition III.8. that hyperinstability is not observed when x_0 is in linear region. Hence, *application of BEM to a linear time-invariant system does not lead to hyperinstability.*

We conclude from Proposition III.9.(ii) that if x_0 is in saturation region, then for a given $A \in \mathbb{R}^{2\times2}$ satisfying either (c) $\frac{|A|}{a_{22}} < 0$ or (d) $|A| > 0$ and $a_{22} = 0$, there exists a lower bound on h such that BEM converges when a value of h exceeding the lower bound is used in the simulation. Consequently, BEM suffers from hyperstability.

C. Discussions and practical recommendations

Based on the analyses presented in sections III-A and III-B, the following conclusions can be drawn.

- (**C1**) If the ground truth of a dynamical system of the form (9) or (12) exhibits global asymptotic convergence, then simulating such a system using BEM with an arbitrarily high stepsize converges to the same equilibrium, thus producing the same end result as in the ground truth while requiring a lower computational effort.
- (**C2**) Simulation using BEM with an arbitrarily high stepsize may lead to hyperstability (in systems of the form (9) or (12)) or hyperinstability (in system of the form (12)). This limits the adoption of arbitrarily high stepsizes during simulation, especially when the A matrix is unknown.

In the context of (C2), the objective is to determine the maximum value of $h = h_M$ such that using $h < h_M$ does not result in hyperstability/hyperinstability. The variable h_M can be easily estimated in some situations. For example, when A has at least one eigenvalue with positive real part, then using $h < h_M = \max\{\frac{2Re(\lambda_i)}{|\lambda_i|^2}\}\ \forall i \in \{1, 2\}$ is sufficient to avoid hyperstability where λ_i is the i^{th} eigenvalue of A. Similarly, analysis of (12) reveals that if $|A| < 0$ and $a_{22} > 0$, then for a certain set of x_0 belonging to the positive saturation region that satisfy $a_{11}c + a_{12}(x_2)_0 > 0$, the ground truth is unstable. Based on the proof of Proposition III.9.(ii), it can be concluded that in such scenarios, using BEM with $h < h_M = \frac{1}{a_{22}}$ is sufficient to avoid hyperstability. However, calculating h_M can be mathematically cumbersome in many situations (for example, when A is Hurwitz). Unless h_M is known, it can be challenging for a power system planner/operator to determine whether the convergence/divergence of the numerical solution is a consequence of hyperstability/hyperinstability or not. Hence,

for practical purposes, we recommend using variable step algorithms over constant step algorithms.

Recently, the authors in [10] presented a BEM-based variable-step algorithm that adapts the stepsize based on two user-defined parameters τ and h_{max}. The value of τ controls the goodness of the initial guess $x_{n+1}^{(0)}$ at $t = t_{n+1}$ in terms of its closeness to the final solution x_{n+1}. On the other hand, h_{max} represents the maximum value of the stepsize that can be adopted by the algorithm. Note that h_{max} need not necessarily be less than h_M. Hence, the knowledge of h_M is not necessary. It has been shown in [7] that by appropriately tuning τ and h_{max}, it is possible to obtain simulation speedup while generating a solution that resembles the ground truth in an averaged sense in many scenarios. As a consequence, appropriate tuning of τ and h_{max} may help in avoiding hyperstability or hyperinstability in systems with saturation nonlinearities while providing computational benefits.

However, similar to any other numerical method, appropriately tuning τ and h_{max} can be challenging. Suppose the system operator has started the simulation by setting up a reasonable value of τ and h_{max}. If the numerical solution converges to an equilibrium, then the operator needs to test the occurrence of hyperstability. Reference [7] presented an approach to detect the occurrence of hyperstability in a power system when the A matrix has at least one eigenvalue with positive real part. In particular, a predictor–corrector approach was proposed in [7] to address the hyperstability issue. The predictor identifies instability based on eigendecomposition of the A matrix at the post-disturbance unstable equilibrium obtained as a byproduct of BEM. The corrector uses the right eigenvectors to identify the group of machines participating in the unstable mode. This helps to apply appropriate protection schemes as in ground truth. However, this approach of detecting hyperstability is not applicable when A is Hurwitz. Since the instability in the ground truth (if any) will be typically non-oscillatory in nature when A is Hurwitz, hyperstability can be avoided by using an algorithm that can track the non-oscillatory instability in the ground truth in an averaged sense. Reference [7] presented an approach wherein, a constant stepsize $h = h_{min}$ (say, 0.002 s) is adopted for a certain number of steps (say r steps) following a power system disturbance. After the r steps, the BEM-based variable stepsize algorithm [10] is invoked with a reasonable choice of τ and h_{max}. This approach was found in [7] to successfully capture the non-oscillatory instability in the ground truth (if any). In a power system with saturation nonlinearity, the probability of the ground truth hitting the saturation is higher immediately after a power system disturbance. As a consequence, limiting the stepsize following a disturbance may prevent the numerical method from producing erroneous solutions in the linear region that may otherwise lead to hyperstability. Hence, in our recommendation, the approach of tracking the non-oscillatory instability presented in [7] can be useful for avoiding hyperstability in systems with saturation nonlinearities when A is Hurwitz. In addition, this approach may help in avoiding hyperinstability which requires further investigation.

IV. Results

The BEM-based variable stepsize algorithm (BEM-VS) [10] is applied to (a) a system with a single synchronous generator (SG) feeding a standalone load and (b) a 6-bus system with a grid-forming converter (GFC), a grid-following converter (GFLC), and a SG. The obtained results are compared with the *ground truths*, which are obtained using the TM-LTE (Local Truncation Error) based variable stepsize algorithm [2]. The parameter tol in the TM-LTE algorithm is set to 0.0001 for accurate reconstruction of the ground truth in the presence of adaptive stepsize variation.

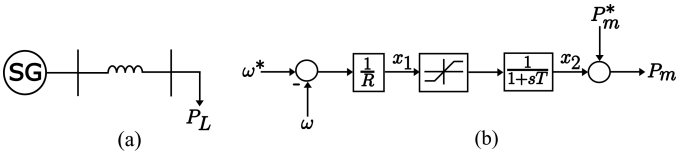

(a) (b)

Fig. 1. (a) Single line diagram of a single SG system feeding a standalone load P_L and (b) Block diagram of the governor's dynamics.

TABLE I
PARAMETERS OF THE SINGLE SG SYSTEM

R	T	c	H	P_m^*	ω^*	ω_s
2.4 Hz/pu	2 s	0.5	5 s	0.5 pu	377 rad/s	377 rad/s

A. Single SG system feeding a standalone load

Figure 1a shows a power system with a single SG feeding a standalone load P_L via a lossless transmission line. The SG is equipped with a governor whose dynamics is shown in Fig. 1b. The variable R is the governor droop and P_m^* is the reference value of the input mechanical power. This system is represented by two state variables: $x_1 = \frac{\Delta\omega}{R}$ (where $\Delta\omega = \omega^* - \omega$ represents the deviation in the SG's speed ω from the reference speed ω^*, measured in electrical rad/s) and $x_2 = \Delta P_m$ (measured in pu) whose dynamics are given by (18)-(19) $\forall\ t \geq 0$.

$$\dot{x_1} = -\frac{\omega_s}{2HR}\left(P_m^* + x_2 - P_L\right) \tag{18}$$

$$\dot{x_2} = -\frac{1}{T}x_2 + \frac{1}{T}\left(c\ \text{sat}\left(\frac{x_1}{c}\right)\right) \tag{19}$$

The variable x_2 is added to P_m^* to obtain the actual input power P_m. Further, throughout this section, $(\frac{\Delta\omega}{R})_{sat} := c\ \text{sat}(\frac{x_1}{c})$. The system parameters are shown in Table I.

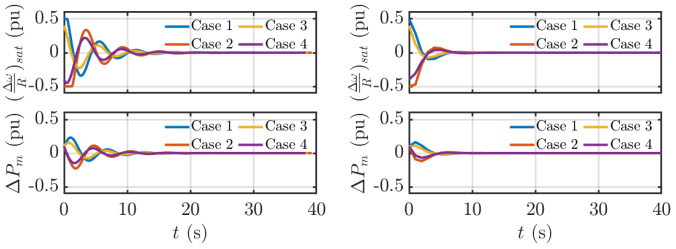

(a) (b)

Fig. 2. (a) Ground truths and (b) outputs from BEM-VS in Cases 1-4.

1) $P_L = P_m^*\ \forall\, t \geq 0$: In this case, the system represented by (18)-(19) can be expressed in the form given by (12). Specifically, the resulting A matrix has the entries $a_{11} = 0$, $a_{12} = -\frac{\omega_s}{2HR}$, $a_{21} = \frac{1}{T}$ and $a_{22} = -\frac{1}{T}$. Clearly, A is Hurwitz and $a_{22} < 0$. Hence, *simulation of this system using BEM cannot lead to hyperinstability* (see Proposition III.9.(ii)). Further, note that the origin of this system is

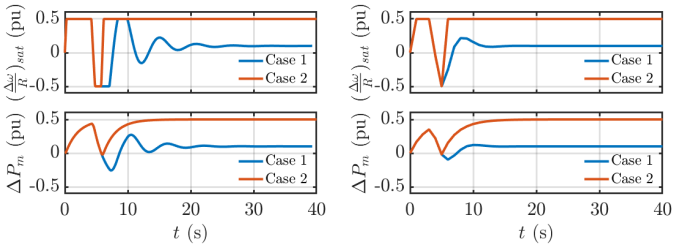

(a) (b)

Fig. 3. (a) Ground truths and (b) outputs from BEM-VS.

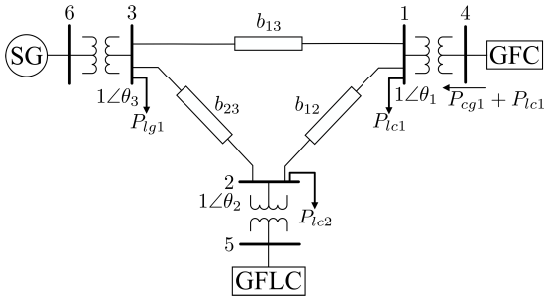

Fig. 4. A 6-bus system with a GFC, a GFLC, and a SG.

globally asymptotically stable (see Proposition III.6.). The BEM-VS algorithm with $\tau = 20$ and $h_{max} = 1$ is applied to simulate this system in four different cases, i.e., Cases 1-4 that correspond to four different initial conditions $x_0 = [0.7\ \ 0.1]^T$ (positive saturation region), $[-0.7\ \ 0.1]^T$ (negative saturation region), $[0.4\ \ 0.1]^T$ (positive linear region), and $[-0.4\ \ 0.1]^T$ (negative linear region) respectively. The obtained results along with the ground truths of Cases 1-4 are shown in Fig. 2 from $t = 0$ to $t = 40$ s.

Owing to global asymptotic stability, the ground truths of Cases 1-4 converge to the origin as shown in Fig. 2a. In addition, it is seen from Fig. 2b that the BEM-VS algorithm also converges to the origin in each of the four cases. *Further, on average, BEM-VS is found to consume* 38.34% *of the time consumed by TM-LTE*. In conclusion, BEM-VS can not only produce the same end result as in the ground truth but also result in a lower computational burden.

2) $P_L \neq P_m^*\ \forall\ t > 0$: In this study, two different cases are considered. In Case 1, a step increase in P_L from 0.5 pu to 1.3 pu is applied at $t = 0$ s followed by a step decrease in P_L from 1.3 pu to 0.2 pu at $t = 2.5$ s, which is again followed by a step increase in P_L from 0.2 pu to 0.6 pu at $t = 5.5$ s. In Case 2, a step increase in P_L from 0.5 pu to 1.3 pu is applied at $t = 0$ s followed by a step decrease in P_L from 1.3 pu to 0.2 pu at $t = 2.5$ s which is again followed by a step increase in P_L from 0.2 pu to 1.5 pu at $t = 5.5$ s. In each of the two Cases 1-2, the system starts from the steady state operating point corresponding to $P_L = 0.5$ pu i.e., $x_0 = [0\ \ 0]^T$. BEM-VS is applied to simulate both the cases with $\tau = 20$ and $h_{max} = 1$. The obtained results along with the ground truths are shown in Fig. 3.

It is seen from Fig. 3a that in Case 1, the ground truth ($(\frac{\Delta\omega}{R})_{sat}$ vs t) converges to the equilibrium (where $(\frac{\Delta\omega}{R})_{sat} = \Delta P_m = 0.1$ pu) after multiple hitting of the saturation limits. Further, we see from Fig. 3b that under the high value of h_{max} and τ used in our experiment, BEM-VS struggles to accurately track the ground truth. However, BEM-VS also converges to the same equilibrium, thus producing the same end result as in the ground truth. *Further, BEM-VS is found to consume* 25.92% *of the time consumed by TM-LTE to converge to the equilibrium.*

On the other hand, it is seen from Fig. 3a that in Case 2, the ground truth ($(\frac{\Delta\omega}{R})_{sat}$ vs t) is unable to return to the linear region after it hits the positive saturation limit for the second time. Hence, this is a case of instability where the mechanical input power to the generator is unable to match the load P_L. Further, since ΔP_m converges to the saturation limit ($= 0.5$ pu), $P_m^* + \Delta P_m - P_L$ converges to -0.5 pu. This implies that eventually, the generator's speed ω decreases linearly with time (see (18)), thus leading to non-oscillatory instability. We see from Fig. 3b that BEM-VS produces a response similar to the ground truth. This implies that BEM-VS is also able to track the non-oscillatory instability of the ground truth in Case 2. In other words, hyperstability is not observed in Case 2 since the system does not have any unstable equilibrium when $P_L = 1.5$ pu. Further, *in Case 2, BEM-VS is found to consume* 28.40% *of the time taken by TM-LTE to produce the unstable trajectory of the generator's speed.* Thus, we conclude that for the single SG system shown in Fig. 1a, BEM-VS can reasonably track both the stability and the non-oscillatory instability of the ground truth even at a high value of h_{max} and τ, while requiring a significantly lower computational effort.

B. 6 bus system with SG, GFC, and GFLC

Figure 4 shows a 6-bus system where a SG is connected to bus 6, a GFC is connected to bus 4 and a GFLC is connected to bus 5. The dynamics of this system can be represented by 7 ODEs and 1 AE [11]. In particular, this system is represented in this paper using seven state variables: v_{dc}, i_{d2}, x_{pll}, ω_3, P_{τ_g}, $X_1 := \theta_1 - \theta_3$ and $X_3 := \theta_{pll} - \theta_3$ along with one algebraic variable $X_2 := \theta_2 - \theta_3$, thus resulting in a 8-dimensional nonlinear DAE system. The reader is referred to [11] for more details about this system along with the notations. The system parameters are also available in [11]. The only difference in our model comes from the real power flows represented using the nonlinear power angle equations.

The initial steady state operating point of this system is $(P_{lc1})_0 = 3$ pu, $(P_{lc2})_0 = 2$ pu, $(P_{lg1})_0 = 3.5$ pu, $(v_{dc})_0 = 1$ pu, $(\theta_1)_0 = -0.0506$ rad, $(i_{d2})_0 = 2$ pu, $(x_{pll})_0 = \omega_s/k_i$ (where $\omega_s = 377$ electrical rad/s and the integral gain of the pll $k_i = 2562$), $(\theta_{pll})_0 = -0.0689$ rad, $(\theta_3)_0 = -0.0873$ rad, $(\omega_3)_0 = \omega_s$, $(P_{\tau_g})_0 = 3$ and $(\theta_2)_0 = -0.0689$ rad. For this study, two cases are considered: (i) a step increase in P_{lc1} from 3 pu to 4.5 pu is applied at $t = 0$ s followed by a step decrease from 4.5 pu to 3 pu at $t = 2$ s; and (ii) a step increase in P_{lc1} from 3 pu to 4.5 pu is applied at $t = 0$ s followed by a step decrease from 4.5 pu to 3 pu at $t = 4$ s. The ground truth is obtained from $t = 0$ to $t = 30$ s in case (i) as shown in Fig. 5a. However, in case (ii), the dc link voltage of the GFC v_{dc} collapses, due to which the ground truth is obtained till 2.7 s only as shown in Fig. 5b. Further, BEM-VS is applied to both case (i) and case (ii) with (a) $\tau = 0.1$, $h_{max} = 1$ and (b) $\tau = 1$, $h_{max} = 1$. The obtained results are shown in Fig. 6 and Fig. 7.

It is seen from Fig. 5a that in case (i), the ground truth (v_{dc} vs t) converges to the equilibrium where $v_{dc} = 1$ pu.

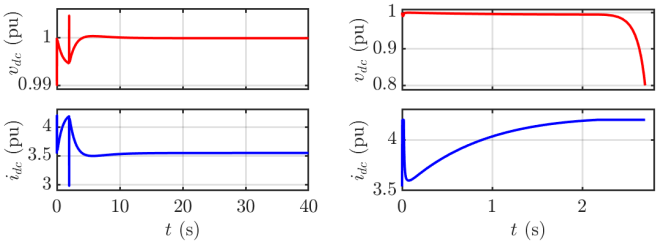

(a) (b)

Fig. 5. Ground truths in (a) case (i) and (b) case (ii).

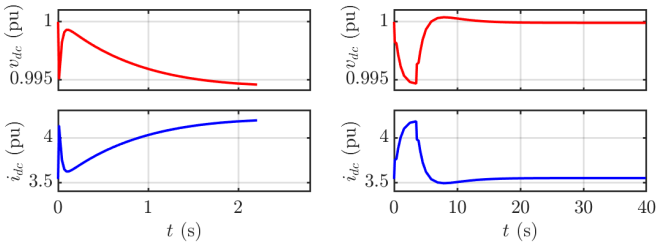

(a) (b)

Fig. 7. Outputs of BEM-VS in case (ii) with (a) $\tau = 0.1$ and (b) $\tau = 1$.

In particular, the dc side current of the GFC i_{dc} just hits the saturation limit ($= 4.2$ pu) when the step decrease in P_{lc1} is applied which prevents the collapse of v_{dc} in this case. We see from Fig. 6 that BEM-VS also converges to the same equilibrium as in the ground truth. *Further, BEM-VS is found to consume* 53.46% *and* 46.81% *of the time taken by TM-LTE to converge to the equilibrium when* $\tau = 0.1$ *and* 1 *respectively.* On the other hand, it is seen from Fig. 7a that BEM-VS is able to capture the collapse of v_{dc} and hence the saturation limit hitting of i_{dc} when $\tau = 0.1$. Additionally, *BEM-VS is found to consume* 58.54% *of the time taken by TM-LTE for predicting the collapse of* v_{dc}*, thus proving to be computationally efficient even in the unstable case.* However, when $\tau = 1$, BEM fails to capture the collapse of v_{dc} as shown in Fig. 7b. In particular, BEM converges to the unstable equilibrium when $\tau = 1$. This is because, when $\tau = 1$, BEM adopts larger time steps in comparison to the setting where $\tau = 0.1$ as shown in Fig. 8. This adoption of larger time steps is leading to hyperstability when $\tau = 1$.

In conclusion, even in a high-dimensional system having saturation nonlinearity, BEM-VS can produce similar end result as in the ground truth at a significantly lower computational cost, if τ and h_{max} are chosen appropriately.

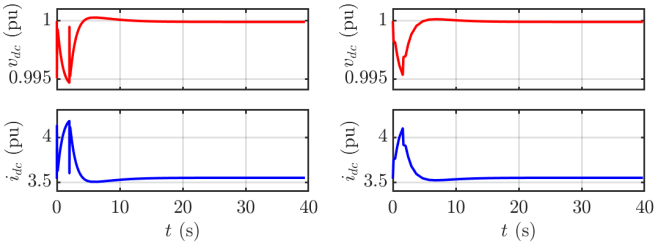

(a) (b)

Fig. 6. Outputs of BEM-VS in case (i) with (a) $\tau = 0.1$ and (b) $\tau = 1$.

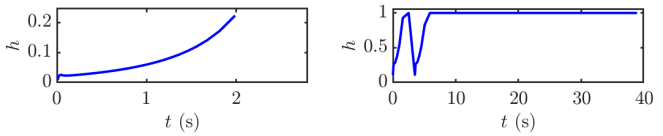

(a) (b)

Fig. 8. (a) Adaptation of the stepsize h of the BEM-VS algorithm in case (ii) with (a) $\tau = 0.1$ and (b) $\tau = 1$.

V. Conclusion

Mathematical analysis is presented in this paper to investigate the applicability of BEM for numerical simulation of dynamical systems with saturation nonlinearity. It is found that BEM can suffer from both hyperstability and hyperinstability in a system with saturation nonlinearity depending on the initial conditions. As a consequence, adaptive stepsize variation is recommended in order to track the ground truth in an averaged sense. A BEM-based variable stepsize algorithm is applied to simulate the dynamics of a governor-equipped single machine system feeding a standalone load. It is found that the algorithm can reasonably track the stability and the non-oscillatory instability of the ground truth, while consuming a significantly lower cpu time. The algorithm is also applied to simulate the dynamics of a 6-bus system connected to inverter based resources. It is found that appropriate tuning of the parameters of the algorithm can not only avoid hyperstability but also capture the dc voltage collapse phenomenon in the 6-bus system, while consuming a cpu time that is significantly lower in comparison to that of the ground truth. In our future works, we will investigate the application of BEM in a large power system with saturation nonlinearities on multiple state variables.

References

[1] P. Kundur, *Power System Stability and Control*. McGraw-Hill, 1994.

[2] D. Griffiths and D. Higham, *Numerical Methods for Ordinary Differential Equations: Initial Value Problems*. Springer, 2010.

[3] P. Henneaux *et al.*, "Benchmarking quasi-steady state cascading outage analysis methodologies," *2018 IEEE Int. Conf. on Prob. Methods Applied to Power Systems (PMAPS)*, pp. 1–6, 2018.

[4] C. J. Mozina, "Undervoltage load shedding," in *2007 60th Annual Conference for Protective Relay Engineers*, 2007, pp. 16–34.

[5] NERC. (2006, Sept.) Guidelines for developing an under voltage load shedding (UVLS) evaluation program.

[6] U. M. Ascher and L. R. Petzold, *Computer methods for ordinary differential equations and differential-algebraic equations*. SIAM, 1998.

[7] S. Gharebaghi, N. R. Chaudhuri, T. He, and T. La Porta, "An approach for fast cascading failure simulation in dynamic models of power systems," *Applied Energy*, vol. 332, p. 120534, 2023.

[8] S. Gharebaghi, N. R. Chaudhuri, T. He, and T. L. Porta, "A method for parallelized fast dynamic cascading failure simulation of power system," in *2023 IEEE Power Energy Society General Meeting (PESGM)*, 2023, pp. 1–5.

[9] P. Deuflhard and F. Bornemann, *Scientific computing with ordinary differential equations*. Springer Science & Business Media, 2012, vol. 42.

[10] D. Fabozzi and T. Van Cutsem, "Simplified time-domain simulation of detailed long-term dynamic models," in *2009 IEEE Power Energy Society General Meeting*, 2009, pp. 1–8.

[11] L. Karunaratne, N. R. Chaudhuri, A. Yogarathnam, and M. Yue, "Nonlinear backstepping control of grid-forming converters in presence of grid-following converters and synchronous generators," *IEEE Transactions on Power Systems*, vol. 39, no. 1, pp. 1948–1964, 2024.